Analytical solution for cylindrical thin shells with normally intersecting nozzles due to external moments on the ends of shells

XUE Mingde (薛明德), WANG Hehui (王和慧), CHEN Wei (陈 伟)
and HUANG Kezhi (HWANG Kehchih, 黄克智)
(Department of Engineering Mechanics, Tsinghua University, Beijing 100084, China)

Received July 25, 1998

Abstract The stress analysis based on the theory of a thin shell is carried out for cylindrical shells with normally intersecting nozzles subjected to external moment loads on the ends of shells with a large diameter ratio ($\rho_0 \leqslant 0.8$). Instead of the Donnell shallow shell equation, the modified Morley equation, which is applicable to $\rho_0(R/T)^{1/2} \gg 1$, is used for the analysis of the shell with cutout. The solution in terms of displacement function for the nozzle with a nonplanar end is based on the Goldenveizer equation. The boundary forces and displacements at the intersection are all transformed from Gaussian coordinates (α, β) on the shell, or Gaussian coordinates (ζ, θ) on the nozzle into three-dimensional cylindrical coordinates (ρ, θ, z). Their expressions on the intersecting curve are periodic functions of θ and expanded in Fourier series. Every harmonic of Fourier coefficients of boundary forces and displacements are obtained by numerical quadrature. The results obtained are in agreement with those from the three-dimensional finite element method and experiments.

Keywords: two normally intersecting cylindrical shells, theory of thin shells, stress concentration factors(SCF).

Two intersecting cylindrical shells subjected to internal pressure and external moments are of common occurrence in pressure vessel and piping industry. The highest stress intensity occurring in the vicinity of junction might cause trouble. The intersecting curve of two cylindrical surfaces, Γ, is a complicated space curve when the diameter ratio of two cylinders increases. Since the 1950s Eringen[1], Bijlaard[2], Qian[3], Lekerkerker[4] and Steele[5] have obtained the analytical solution for $\rho_0 = r/R \leqslant 0.3$ based on the Donnell's shallow shell equation and on the supposition that Γ is a circle laid on the developed surface of the main shell[1)]. Since the 1980s Moffat[6,7] and Widera[8] have been making efforts to obtain FEM solution and to develop empirical formulas on numerical and experimental results. The authors and co-workers of the present paper developed a thin shell theoretical solution of two normally intersecting cylindrical shells subjected to internal pressure[9—13]. The solution is developed from the symmetrical case into the asymmetrical cases about $\theta = 0$, $\pi/2$ and from Timoshenko's solution[14] into Goldenveizer's solution[15] for branch pipes in this paper. Usually two intersecting cylindrical shells are subjected to arbitrary kinds of external load accompanied with internal pressure. An arbitrary external moment loaded to the main shell could be decomposed into three basic moments, that is, torsional moment, M_{xc}, longitudinal moment, M_{yc}, and transverse moment, M_{zc}, as shown in fig. 1. For this problem the governing differential equations and the analytical solutions are given in the present paper.

1) Steele[5] gave an approximate solution suited for $\rho_0 \leqslant 0.5$.

The geometric parameters and four coordinate systems are shown in fig. 1. The Cartesian and polar coordinate systems (ξ, φ) and (α, β) on the developed surface of the main shell and the Cartesian (ζ, θ) on the developed surface of branch pipe are taken as Gaussian coordinates, respectively. Cylindrical coordinates (ρ, θ, z) are taken as the global system. Their transformations are shown in references [9—13].

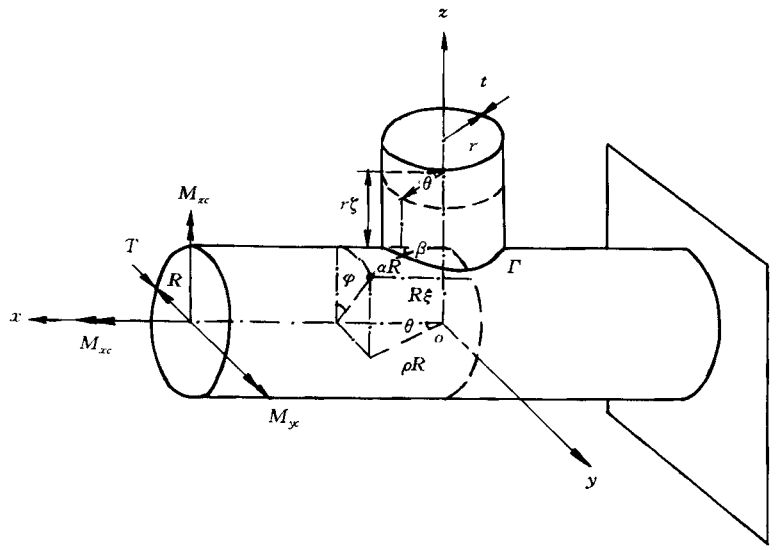

Fig. 1. Four-coordinate systems.

Three loading cases based on symmetrical or antisymmetrical stress fields about $\theta = 0 (\beta = 0)$ and $\theta = \pi/2$ $(\beta = \pi/2)$ caused by themselves, are given in table 1. All components of force, moment, deformation and displacement can be expanded in Fourier series of β (or θ). For example, the set of complete trigonometric functions of membrane normal forces, T_α and T_β, bending moments, M_α and M_β, and transverse shear force, Q_α, is marked by $(G_N^{(1)}(m\beta)$ (or $G_N^{(1)}(m\theta))$ and those of membrane shear force $T_{\alpha\beta}$, torsion moment $M_{\alpha\beta}$ and transverse shear force, Q_β, $G_N^{(2)}(m\beta)$ (or $G_N^{(2)}(m\theta))$, where m is harmonic number, and subscript $N = 1, 2, 3$ is the case number. The subscript of general forces, α and β, is transformed into ζ and θ for branch pipe respectively. $G_N^{(1)}(m\beta)$ and $G_N^{(2)}(m\beta)$ for each case are shown in table 1.

Table 1 Symmetry and trigonometric functions in three cases

Case	About $\beta = 0$	About $\beta = \pi/2$	$G_N^{(1)}(m\beta)$	$G_N^{(2)}(m\beta)$	Loading
$N = 1$	symmetry	symmetry	$\cos 2k\beta$	$\sin 2k\beta$	M_{yc}
$N = 2$	antisymmetry	antisymmetry	$\sin 2k\beta$	$-\cos 2k\beta$	M_{xc}
$N = 3$	antisymmetry	symmetry	$\sin(2k+1)\beta$	$-\cos(2k+1)\beta$	M_{zc}

1 Thin shell theoretical solution of cylindrical shell with large opening due to external moments on its ends

The solution is obtained by superposition of membrane solution on homogeneous solution. Membrane solution is given in Cartesian coordinates, (ξ, φ), and homogeneous in polar, (α, β).

Homogeneous solution based on modified Morley's equation with the accuracy order of $O(T/R)$, which is the accuracy of thin shell theory, can be applied to large openings.

1.1 Membrane solution

Under the torsional moment M_{xc}:

$$\hat{T}_{\xi\varphi} = \frac{M_{xc}}{2\pi R^2}, \quad \hat{T}_{\xi} = \hat{T}_{\varphi} = 0, \tag{1a, b}$$

$$\hat{u}_{\varphi} = \frac{2(1+\nu)}{ET}\frac{M_{xc}}{2\pi R}\xi. \tag{2}$$

Under the in-plane bending moment M_{yc},

$$\hat{T}_{\xi} = \frac{M_{yc}}{\pi R^2}\cos\varphi, \quad \hat{T}_{\varphi} = \hat{T}_{\xi\varphi} = 0, \tag{3a, b}$$

$$\hat{u}_{\xi} = \frac{M_{yc}}{ET\pi R}\xi\cos\varphi, \quad \hat{u}_{\varphi} = \frac{M_{yc}}{2ET\pi R}\left(\xi^2 - \frac{L^2}{R^2}\right)\sin\varphi, \tag{4a, b}$$

$$\hat{u}_n = -\frac{M_{yc}}{ET\pi R}\left[\nu + \frac{1}{2}\left(\xi^2 - \frac{L^2}{R^2}\right)\right]\cos\varphi, \tag{4c}$$

$$\hat{\gamma}_{\xi} = -\frac{M_{yc}}{ET\pi R^2}\xi\cos\varphi, \quad \hat{\gamma}_{\varphi} = \frac{\nu M_{yc}}{ET\pi R^2}\sin\varphi. \tag{5a, b}$$

Under the out-plane bending moment M_{zc},

$$\hat{T}_{\xi} = -\frac{M_{zc}}{\pi R^2}\sin\varphi, \quad \hat{T}_{\varphi} = \hat{T}_{\xi\varphi} = 0, \tag{6a, b}$$

$$\hat{u}_{\xi} = -\frac{M_{zc}}{ET\pi R}\xi\sin\varphi, \quad \hat{u}_{\varphi} = \frac{M_{zc}}{2ET\pi R}\left(\xi^2 - \frac{L^2}{R^2}\right)\cos\varphi, \tag{7a, b}$$

$$\hat{u}_n = \frac{M_{zc}}{ET\pi R}\left[\nu + \frac{1}{2}\left(\xi^2 - \frac{L^2}{R^2}\right)\right]\sin\varphi, \tag{7c}$$

$$\hat{\gamma}_{\xi} = \frac{M_{zc}}{ET\pi R^2}\xi\sin\varphi, \quad \hat{\gamma}_{\varphi} = \frac{\nu M_{zc}}{ET\pi R^2}\cos\varphi. \tag{8a, b}$$

1.2 Homogeneous solution

The modified Morley's equation

$$\left(\nabla^2 + \frac{1}{2} + 2\mu\sqrt{i}\frac{\partial}{\partial\xi}\right)\left(\nabla^2 + \frac{1}{2} - 2\mu\sqrt{i}\frac{\partial}{\partial\xi}\right)\chi = 0 \tag{9}$$

is used instead of Donnell's shallow shell equation used in refs. [1—5].

$$\left(\nabla^2 + 2\mu\sqrt{i}\frac{\partial}{\partial\xi}\right)\left(\nabla^2 - 2\mu\sqrt{i}\frac{\partial}{\partial\xi}\right)\chi = 0, \tag{10}$$

where

$$\chi = u_n + i\frac{4\mu^2}{ETR}\phi, \tag{11}$$

where the real part of χ, u_n is the normal displacement; the imaginary part ϕ is the Airy stress function and

$$4\mu^2 = [12(1-\nu^2)]^{1/2}R/T. \tag{12}$$

The solution of eq. (9) for the three cases shown in table 1 can be obtained as in reference [4].

$$\chi = \sum_{k=e(4,N)}^{\infty}\sum_{n=e(1,N)}^{\infty} C_n F_{kn}(\alpha) G_N^{(1)}(m\beta), \tag{13}$$

where C_n are unknown complex constants,

$$C_n = C_{n1} + iC_{n2}; \tag{14}$$

m is harmonic number

$$m = 2k + e(2, N); \tag{15}$$

$G_N^{(1)}(m\beta)$ is trigonometric functions shown in table 1 and

$$F_{kn} = (-1)^k\left(1 - \frac{1}{2}\delta_{m0}\right)\left[J_{m-n}(\sqrt{-i}\mu\alpha) + e(3, N)J_{-m-n}(\sqrt{-i}\mu\alpha)\right]H_n(\eta\alpha), \tag{16}$$

where J_n and H_n are nth-order Bessel and Hankel functions respectively. $e(1, N)\sim e(4, N)$ are given in table 2 and

$$\delta_{km} = \begin{cases} 0, & k \neq m, \\ 1, & k = m, \end{cases} \tag{17}$$

$$\eta = \left(\frac{1}{2} - i\mu^2\right)^{1/2}. \tag{18}$$

Table 2 $e(j, N)$ in three cases

Case	$e(1, N)$	$e(2, N)$	$e(3, N)$	$e(4, N)$
$N=1$	0	0	1	0
$N=2$	1	0	−1	1
$N=3$	1	1	1	0

The components of membrane forces, T_α, T_β, $T_{\alpha\beta}$ are expressed through the imaginary part of χ and moments, M_α, M_β, $M_{\alpha\beta}$, and transverse shear forces, Q_α, Q_β, through the real part (see eqs. (11)—(18) in ref. [9]). The components of tangential deformation, ε_α, ε_β, ω, can be obtained from constitutive equations in the tangential plane of shell. Then the Fourier coefficients of expressions of partial derivative of u_α, u_β with respect to α, β, $f_k(\alpha)$ $g_k(\alpha)$ and $h_k(\alpha)$, can be obtained from geometrical description of thin shell theory[16]:

$$\frac{1}{R}\frac{\partial u_\alpha}{\partial \alpha} = \frac{1}{ET}(T_\alpha - \nu T_\beta) - \frac{u_n}{R}\sin^2\beta = \sum_{k=0}^{\infty} f_k(\alpha)G_N^{(1)}(m\beta), \tag{19a}$$

$$\frac{1}{\alpha R}\frac{\partial u_\beta}{\partial \beta} + \frac{1}{R}\frac{u_\alpha}{\alpha} = \frac{1}{ET}(T_\beta - \nu T_\alpha) - \frac{u_n}{R}\cos^2\beta = \sum_{k=0}^{\infty} g_k(\alpha)G_N^{(1)}(m\beta), \tag{19b}$$

$$\frac{1}{R}\left(\frac{1}{\alpha}\frac{\partial u_\alpha}{\partial \beta} + \frac{\partial u_\beta}{\partial \alpha} - \frac{u_\beta}{\alpha}\right) = \frac{2(1+\nu)}{ET}T_{\alpha\beta} - \frac{u_n}{R}\sin 2\beta = \sum_{k=e(4,N)}^{\infty} h_k(\alpha)G_N^{(2)}(m\beta), \tag{19c}$$

and u_α, u_β can be expanded in Fourier series as follows:

$$u_\alpha = \sum_{k=0}^{\infty} U_k(\alpha)G_N^{(1)}(m\beta), \quad u_\beta = \sum_{k=e(4,N)}^{\infty} V_k G_N^{(2)}(m\beta). \tag{20}$$

Substituting eq. (20) into eq. (19), we can get a set of differential equations and obtain the solution for each k:

$$U_k = \alpha R\left(f_k - \alpha\frac{\mathrm{d}g_k}{\mathrm{d}\alpha} + mh_k\right)/(1 - m^2), \quad k > 0, \tag{21a}$$

$$V_k = (\alpha R g_k - U_k)/m, \quad k > 0. \tag{21b}$$

Considering that the rigid body displacement causes zero stress field, U_0 and V_0 can be determined based on zero rigid body displacement for case $N=1$ and case $N=3$ as follows (U_0 and V_0 vanish in case 2).

When $N=1$, because the rigid rotation round z-axis is zero, we have

$$U_0 = \alpha R g_0, \quad V_0 = 0. \tag{22a}$$

When $N=3$, because the rigid displacement in the direction of y is zero, we have

$$U_0 = V_0 = \frac{1}{2}\alpha R g_0. \tag{22b}$$

1.3 General forces and displacements at the edge of the hole in the main shell

The expressions for the intersecting curve Γ in the system (α, β) are

$$\alpha_\Gamma = [\rho_0^2\cos^2\theta + \arcsin^2(\rho_0\sin\theta)]^{1/2}, \tag{23a}$$

$$\beta_\Gamma = \arcsin\{\arcsin(\rho_0\sin\theta)[\rho_0^2\cos^2\theta + \arcsin^2(\rho_0\sin\theta)]^{-\frac{1}{2}}\}, \tag{23b}$$

and the homogeneous solutions of general forces and displacements on Γ can be given by substituting eq. (23 a, b) into their expressions. The particular solutions on Γ are obtained by substituting $(\xi_\Gamma, \varphi_\Gamma)$ into their formulas, where ξ_Γ and φ_Γ are the Cartesian coordinates of Γ

$$\xi_\Gamma = \rho_0\cos\theta, \quad \varphi_\Gamma = \arcsin(\rho_0\sin\theta). \tag{24a, b}$$

The tangential forces, T_ν and S_ν, and transverse shear force, Q_ν, which are the components of boundary force vector $\boldsymbol{F}$, and bending moment, M_ν, on boundary Γ, are expressed in the direction of triad of unit vectors at the hole edge $(\boldsymbol{i}_t, \boldsymbol{i}_\nu, \boldsymbol{i}_n)$. The boundary displacement vector, $\boldsymbol{U}$ and γ_ν at the hole edge is composed of u_α, u_β, u_n and γ_α, γ_β, respectively, as shown in fig. 2. The relation between $(\boldsymbol{i}_t, \boldsymbol{i}_\nu, \boldsymbol{i}_n)$ and $(\boldsymbol{i}_\alpha, \boldsymbol{i}_\beta)$ shown in ref. [12] are periodic functions of θ and dependent on parameter ρ_0. $\boldsymbol{F}$ and $\boldsymbol{U}$ are re-decomposed in the global coordinates and F_ρ, F_θ, F_z, M_ν, u_ρ, u_θ, u_z, γ_ν are the eight basic general forces and displacements at the hole edge of the main shell. They are expanded in Fourier series of θ and dependent on diameter ratio ρ_0 and real and imaginary parts of unknown complex constants, $C_{nl}(l=1,2)$. For example,

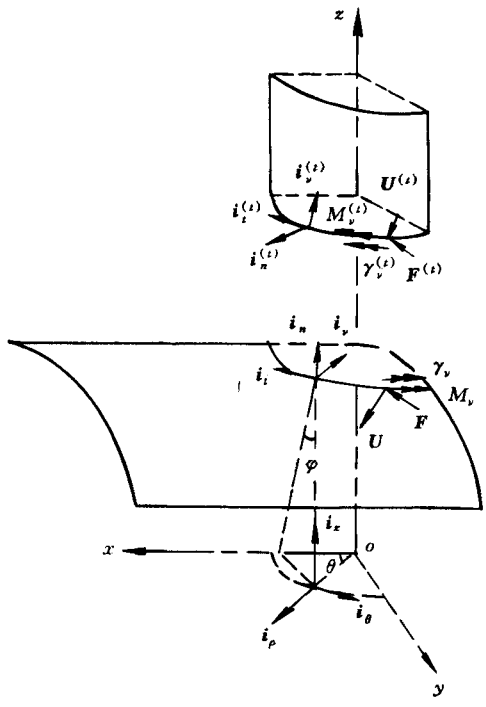

Fig. 2. The directions of unit vector boundary forces and displacements on Γ.

$$F_\rho = \sum_{k=0}^{\infty}\left\{\sum_{n=e(1,N)}^{\infty}\sum_{l=1}^{2} C_{nl} f_{knl}^{\rho}(\rho_0) + \tilde{f}_k^{\rho}(\rho_0)\right\} G_N^{(1)}(m\theta), \tag{25a}$$

$$F_\theta = \sum_{k=0}^{\infty}\left\{\sum_{n=e(1,N)}^{\infty}\sum_{l=1}^{2} C_{nl} f_{knl}^{\theta}(\rho_0) + \tilde{f}_k^{\theta}(\rho_0)\right\} G_N^{(2)}(m\theta), \tag{25b}$$

$$F_z = \sum_{k=0}^{\infty}\left\{\sum_{n=e(1,N)}^{\infty}\sum_{l=1}^{2} C_{nl} f_{knl}^{z}(\rho_0) + \tilde{f}_k^{z}(\rho_0)\right\} G_N^{(1)}(m\theta), \tag{25c}$$

$$M_\nu = \sum_{k=0}^{\infty}\left\{\sum_{n=e(1,N)}^{\infty}\sum_{l=1}^{2}C_{nl}f_{knl}^{m}(\rho_0)+\hat{f}_k^{m}(\rho_0)\right\}G_N^{(1)}(m\theta), \tag{25d}$$

$$u_\rho = \sum_{k=0}^{\infty}\left\{\sum_{n=e(1,N)}^{\infty}\sum_{l=1}^{2}C_{nl}u_{knl}^{\rho}(\rho_0)+\hat{u}_k^{\rho}(\rho_0)\right\}G_N^{(1)}(m\theta), \tag{26a}$$

$$u_\theta = \sum_{k=e(4,N)}^{\infty}\left\{\sum_{n=e(1,N)}^{\infty}\sum_{l=1}^{2}C_{nl}u_{knl}^{\theta}(\rho_0)+\hat{u}_k^{\theta}(\rho_0)\right\}G_N^{(2)}(m\theta), \tag{26b}$$

$$u_z = \sum_{k=0}^{\infty}\left\{\sum_{n=e(1,N)}^{\infty}\sum_{l=1}^{2}C_{nl}u_{knl}^{z}(\rho_0)+\hat{u}_k^{z}(\rho_0)\right\}G_N^{(1)}(m\theta), \tag{26c}$$

$$\gamma_\nu = \sum_{k=0}^{\infty}\left\{\sum_{n=e(1,N)}^{\infty}\sum_{l=1}^{2}C_{nl}u_{knl}^{m}(\rho_0)+\hat{u}_k^{m}(\rho_0)\right\}G_N^{(1)}(m\theta), \tag{26d}$$

where the first items are homogeneous solutions and the second items particular solutions. $f_{knl}^{\rho}\cdots$, $\hat{f}_k^{\rho}\cdots$, $u_{knl}^{\rho}\cdots$, $\hat{u}_k^{\rho}\cdots$ are Fourier coefficients that are definite integrals in which integrands are very complicated expressions involving Bessel and Hankel functions shown in eq. (16) and trigonometrical functions such as eqs. (23) and (24). They are calculated by numerical quadrature[12].

2 The homogeneous solution for a closed cylindrical shell with curved ends

2.1 Goldenveizer general solution[15] for a closed cylindrical shell

Branch pipe is a semi-infinite long circular pipe with a curved end (radius is r, thickness is t). The expressions of components of displacement for branch pipe, $u_\rho^{(t)}$, $u_\theta^{(t)}$ and $u_\zeta^{(t)}$, through displacement function, $\psi(\zeta,\theta)$, are

$$u_\rho^{(t)} = \left\{\nabla^4 + a^2\left[4\frac{\partial^4}{\partial\zeta^4}+\frac{2(2-2\nu+\nu^2)}{1-\nu}\frac{\partial^4}{\partial\zeta^2\partial\theta^2}+\frac{\partial^4}{\partial\theta^4}\right]\right\}\psi, \tag{27a}$$

$$u_\theta^{(t)} = -\frac{\partial}{\partial\theta}\left\{\frac{\partial^2}{\partial\theta^2}+(2+\nu)\frac{\partial^2}{\partial\zeta^2}-a^2\left[\frac{2(2-\nu)}{1-\nu}\frac{\partial^4}{\partial\zeta^4}+\frac{4-3\nu+\nu^2}{1-\nu}\frac{\partial^4}{\partial\theta^2\partial\zeta^2}+\frac{\partial^4}{\partial\theta^4}\right]\right\}\psi, \tag{27b}$$

$$u_\zeta^{(t)} = \frac{\partial}{\partial\zeta}\left\{\frac{\partial^2}{\partial\theta^2}-\nu\frac{\partial^2}{\partial\zeta^2}-a^2\left[\frac{(1+\nu)(2+\nu)}{1-\nu}\frac{\partial^4}{\partial\theta^2\partial\zeta^2}+\frac{1+\nu}{1-\nu}\frac{\partial^4}{\partial\theta^4}+4\nu\frac{\partial^2}{\partial\zeta^2}+\frac{2\nu^2}{1-\nu}\frac{\partial^2}{\partial\theta^2}\right]\right\}\psi, \tag{27c}$$

where

$$a^2 = t^2/12r^2.$$

The governing equation of cylindrical shells expressed through $\psi(\zeta,\theta)$ is

$$\nabla^8\psi + 4\lambda_t^4\frac{\partial^4\psi}{\partial\zeta^4}+(8-2\nu^2)\frac{\partial^6\psi}{\partial\zeta^4\partial\theta^2}+8\frac{\partial^6\psi}{\partial\zeta^2\partial\theta^4}+2\frac{\partial^6\psi}{\partial\theta^6}+4\frac{\partial^4\psi}{\partial\zeta^2\partial\theta^2}+\frac{\partial^4\psi}{\partial\theta^4}=0, \tag{28}$$

where

$$\nabla^2 = \frac{\partial^2}{\partial\theta^2}+\frac{\partial^2}{\partial\zeta^2}, \qquad \lambda_t = [3(1-\nu^2)r^2/t^2]^{1/4}. \tag{29}$$

For three different cases shown in table 1, $\psi(\zeta,\theta)$ is expanded in Fourier series of θ as follows:

$$\psi = \sum_{k=e(4,N)}^{\infty}\sum_{l=1}^{4}D_{kl}g_{ml}(\zeta)G_N^{(1)}(m\theta). \tag{30}$$

The characteristic equation of eq. (28) can be simplified according to the analysis of its characteristic roots by Goldenveizer[15], so we get

$$g_{m1}(\zeta) = \begin{cases} 0, & m = 0, \\ 1, & m = 1, \\ e^{-a_{m1}\zeta}\cos b_{m1}\zeta, & m > 1, \end{cases} \tag{31a}$$

$$g_{m2}(\zeta) = \begin{cases} 0, & m = 0, \\ \zeta, & m = 1, \\ e^{-a_{m1}\zeta}\sin b_{m1}\zeta, & m > 1, \end{cases} \tag{31b}$$

$$g_{m3}(\zeta) = e^{-a_{m2}\zeta}\cos b_{m2}\zeta, \tag{31c}$$

$$g_{m4}(\zeta) = e^{-a_{m2}\zeta}\sin b_{m2}\zeta, \tag{31d}$$

where

$$a_{m1} = b_{m1} = m\sqrt{m^2 - 1}/(2\lambda_t), \qquad 1 < m < \lambda_t, \tag{32a}$$

$$\left.\begin{aligned} a_{m1} &= \left(-\lambda_t + \sqrt{\sqrt{4m^4 + \lambda_t^4} + 2m^2}\right)/2 \\ b_{m1} &= \left(-\lambda_t + \sqrt{\sqrt{4m^4 + \lambda_t^4} - 2m^2}\right)/2 \end{aligned}\right\}, \qquad m \geqslant \lambda_t, \tag{32b}$$

$$a_{m2} = b_{m2} = \lambda_t, \qquad m = 0, \tag{33a}$$

$$a_{m2} = \sqrt{\lambda_t^2 + 1},\ b_{m2} = \sqrt{\lambda_t^2 - 1}, \quad m = 1, \tag{33b}$$

$$a_{m2} = b_{m2} = \lambda_t, \qquad 1 < m < \lambda_t, \tag{33c}$$

$$\left.\begin{aligned} a_{m2} &= \left(\lambda_t + \sqrt{\sqrt{4m^4 + \lambda_t^4} + 2m^2}\right)/2 \\ b_{m2} &= \left(\lambda_t + \sqrt{\sqrt{4m^4 + \lambda_t^4} - 2m^2}\right)/2 \end{aligned}\right\}, \qquad m \geqslant \lambda_t. \tag{33d}$$

Eqs. (32) and (33c, d) are approximate formulas with the accuracy order of $O(m^2 t/r)$ for eqs. (32a), (33c) and $O(1/m^2)$ for equations (32b) and (33d).

The solutions for branch pipe only have homogeneous parts when the external moments are only loaded on the ends of main shell, so the displacement fields in branch pipe can be obtained by eq. (27) and the stress fields by geometrical relations and constitutive equations[16].

2.2 The general forces and displacements at the curve end of branch pipe

The geometric description of the intersecting curve, Γ, in the developed surface of branch pipe is

$$\zeta_\Gamma(\theta) = \frac{1}{\rho_0}(1 - \rho_0^2\sin^2\theta)^{1/2} = \zeta_\Gamma(\rho_0, \theta). \tag{34}$$

From eqs. (30), (31), (27) and (34) we can see that all general forces and displacements are the functions of $(\zeta_\Gamma(\rho_0, \theta), \theta)$, that is, the periodic functions of θ, and dependent on ρ_0 and unknown constants D_{kl}. Therefore, they can be expanded in Fourier series and the Fourier coefficients can be calculated by numerical integration as well.

3 Continuity conditions

At the intersecting curve, the general forces and displacements of the main shell and branch pipe must satisfy the following continuity conditions:

$$F_\rho = -F_\rho^{(t)},\ F_\theta = -F_\theta^{(t)},\ F_z = -F_z^{(t)},\ M_\nu = M_\nu^{(t)}, \tag{35a}$$

$$u_\rho = u_\rho^{(t)},\ u_\theta = u_\theta^{(t)},\ u_z = u_z^{(t)},\ \gamma_\nu = -\gamma_\nu^{(t)}. \tag{35b}$$

Substituting eqs. (25)—(27) and (30), truncated after the terms of either $k = K$ or $n =$

$2K + e(2, N)$ into eq. (35), from eqs. (13)—(15), (30)—(31) and tables 1 and 2 we can see that the number of unknown constants C_{nl} and D_{jl} for three different cases is shown in table 3.

Table 3 Number of constants in three cases

Case	C_{nl}	D_{jl}
$N=1$	$4K+2$	$4K+2$
$N=2$	$4K$	$4K$
$N=3$	$4K+2$	$4K+2$

From eqs. (35a, b), we can get the following equations for each harmonic Fourier coefficient:

$$\sum_{n=e(1,N)}^{2K+e(2,N)}\sum_{l=1}^{2} C_{nl} f^{\rho}_{knl} + \hat{f}^{\rho}_{k} = -\sum_{j=e(4,N)}^{K}\sum_{l=1}^{4} D_{jl} f^{(t)\rho}_{kjl}, \qquad k = e(4,N), \cdots, K, \tag{36a}$$

$$\sum_{n=e(1,N)}^{2K+e(2,N)}\sum_{l=1}^{2} C_{nl} f^{\theta}_{knl} + \hat{f}^{\theta}_{k} = -\sum_{j=e(4,N)}^{K}\sum_{l=1}^{4} D_{jl} f^{(t)\theta}_{kjl}, \qquad k = 0, \cdots, K, \tag{36b}$$

$$\sum_{n=e(1,N)}^{2K+e(2,N)}\sum_{l=1}^{2} C_{nl} f^{z}_{knl} + \hat{f}^{z}_{k} = -\sum_{j=e(4,N)}^{K}\sum_{l=1}^{4} D_{jl} f^{(t)z}_{kjl}, \qquad k = e(4,N), \cdots, K, \tag{36c}$$

$$\sum_{n=e(1,N)}^{2K+e(2,N)}\sum_{l=1}^{2} C_{nl} f^{m}_{knl} + \hat{f}^{m}_{k} = \sum_{j=e(4,N)}^{K}\sum_{l=1}^{4} D_{jl} f^{(t)m}_{kjl}, \qquad k = e(4,N), \cdots, K, \tag{36d}$$

$$\sum_{n=e(1,N)}^{2K+e(2,N)}\sum_{l=1}^{2} C_{nl} u^{\rho}_{knl} + \hat{u}^{\rho}_{k} = \sum_{j=e(4,N)}^{K}\sum_{l=1}^{4} D_{jl} u^{(t)\rho}_{kjl}, \qquad k = e(4,N), \cdots, K, \tag{37a}$$

$$\sum_{n=e(1,N)}^{2K+e(2,N)}\sum_{l=1}^{2} C_{nl} u^{\theta}_{knl} + \hat{u}^{\theta}_{k} = \sum_{j=e(4,N)}^{K}\sum_{l=1}^{4} D_{jl} u^{(t)\theta}_{kjl}, \qquad k = e(4,N), \cdots, K, \tag{37b}$$

$$\sum_{n=e(1,N)}^{2K+e(2,N)}\sum_{l=1}^{2} C_{nl} u^{z}_{knl} + \hat{u}^{z}_{k} = \sum_{j=e(4,N)}^{K}\sum_{l=1}^{4} D_{jl} u^{(t)z}_{kjl}, \qquad k = e(4,N), \cdots, K, \tag{37c}$$

$$\sum_{n=e(1,N)}^{2K+e(2,N)}\sum_{l=1}^{2} C_{nl} u^{m}_{knl} + \hat{u}^{m}_{k} = -\sum_{j=e(4,N)}^{K}\sum_{l=1}^{4} D_{jl} u^{(t)m}_{kjl}, \qquad k = e(4,N), \cdots, K. \tag{37d}$$

Test-calculation shows that the truncation error for stress concentration factors is less than 1% when $K=5$ or 6. From eqs. (13)—(15) and (30)—(31) and tables 1, 2 we can get the number of unknown constants C_{nl} and D_{jl} shown in table 3 for three different cases. The reason is

Case 1. When $k=0$, there are no eqs. (36b) and (37b). Eq. (36c) expressing equilibrium of forces in the direction of z axis should be auto-satisfied; and eq. (37c) expressing the continuity of rigid-body displacements in z-direction, is unnecessary to be considered because it has no effect on stress fields; so the number of independent equations is $8K+4$.

Case 2. When $k=0$, there is only eq. (36b) expressing torsion equilibrium about rotational axis (z-axis), which is auto-satisfied. So the number of equations is $8K$.

Case 3. When $k=0(m=1)$, because the equilibrium of forces and moments should be auto-satisfied, the 4 conditions $F_x = F_z = M_y = M_z = 0$ are auto-satisfied due to symmetric functions $G_N^{(2)}(m\theta)(N=3)$ about $y=0$ and antisymmetric $G_N^{(1)}(m\theta)(N=3)$ about $x=0$. The following equation

$$\oint (F_\rho \sin\theta + F_\theta \cos\theta)\mathrm{d}s_\Gamma = 0 \tag{38}$$

must be auto-satisfied due to $F_y=0$ so that only one equation of eq. (36a, b) is independent.

$$M_x = \oint [F_z\rho_0\sin\theta - M_\nu\cos(i_t, i_x)]\mathrm{d}s_\Gamma \tag{39}$$

should be auto-satisfied due to the moment equilibrium about x-axis so that only one equation of eq. (36c, d) is independent.

As to the condition of rigid-body displacement when $k=0$ ($m=1$), the four conditions $u_x^{(0)} = u_z^{(0)} = \omega_y^{(0)} = \omega_z^{(0)} = 0$ are auto-satisfied and the continuity conditions of $u_y^{(0)}$, $\omega_x^{(0)}$ can be omitted because they have no effect on stress fields.

Notice

$$u_y^{(0)} = \oint (u_\rho\sin\theta + u_\theta\cos\theta)\mathrm{d}s_\Gamma, \tag{40a}$$

$$\omega_x^{(0)} = -\oint \left[\frac{1}{R}(u_\rho\sin\theta\cos\varphi + u_\theta\cos\theta\cos\varphi - u_z\sin\varphi) + \gamma_\nu\cos(i_t, i_a)\right]\mathrm{d}s_\Gamma, \tag{40b}$$

so that eqs. (37b) and (37c) can be omitted. Therefore, for case 3 eqs. (36a), (36d), (37a) and (37d) are used only and we have $8K+4$ independent equations.

4 Verification

4.1 Comparison of tested results for ORNL-1[17] ($\rho_0=0.5$, $D/T=d/t=100$)

The comparison of tested results for ORNL-1 model shown in figs. 3 and 4 shows that the

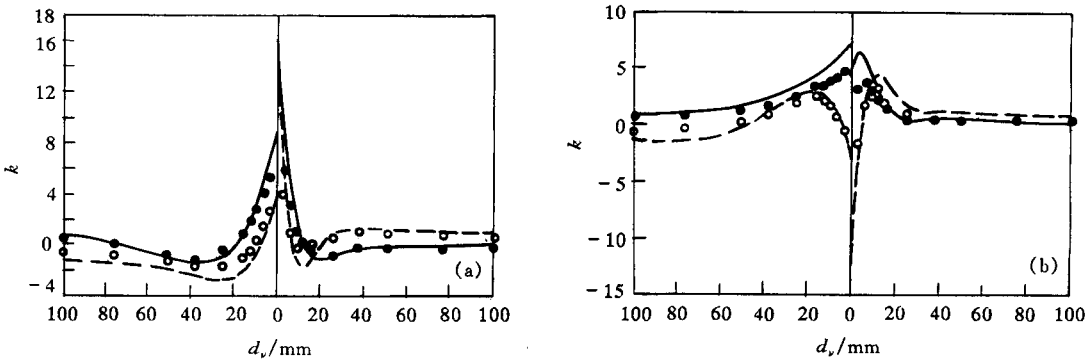

Fig. 3. (a) Distribution of k along the gage line $\theta=60°$ on the outer surface of model ORNL-1 for M_{xc}. (b) Distribution of k along the gage line $\theta=60°$ on the inner surface of model ORNL-1 for M_{xc}. - - -, k_ν analytic; —, k_t analytic.

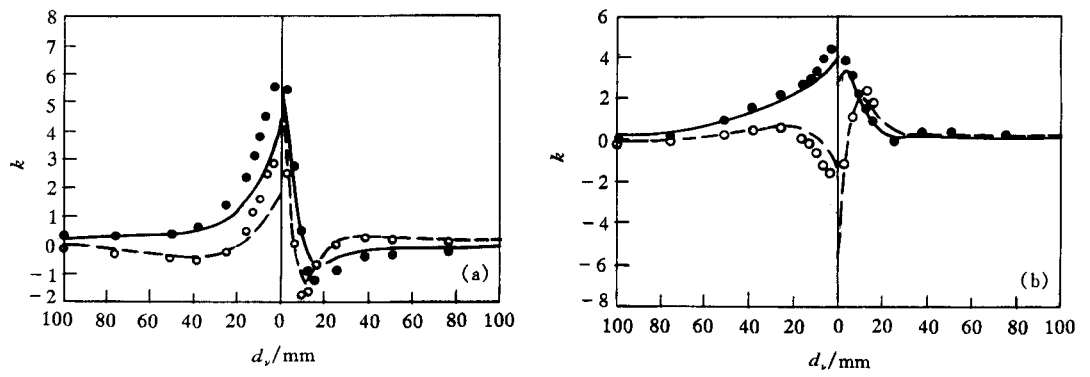

Fig. 4. (a) Distribution of k along the gage line $\theta=90°$ on the outer surface of model ORNL-1 for $M_{x\theta}$. (b) Distribution of k along the gage line $\theta=90°$ on the inner surface of model ORNL-1 for $M_{x\theta}$. ○, k_ν tested; ●, k_t tested.

present theoretical results are in good agreement with the tested one for the loading cases of tor-

sion (main shell subjected to M_{xc}) and in-plane bending (which subjected to M_{yc}). However, for the cases of out-plane bending (loaded by M_{zc}) the tested results are different from the present results just as they are different from FEM results as shown in ref. [17]. Ref. [17] did not explain the reason but the present and numerical results are in good agreement with each other for the out-plane bending cases. Take an example for large diameter ratio as shown in figure 5.

In figs. 3—5 k_t and k_ν are dimensionless normal stresses in the inner or outer surface of the main shell and the subscripts t and ν mean the stress directions in i_t and i_ν, respectively. d_ν is the normal distance from a described point to Γ on the developed surface of the main shell.

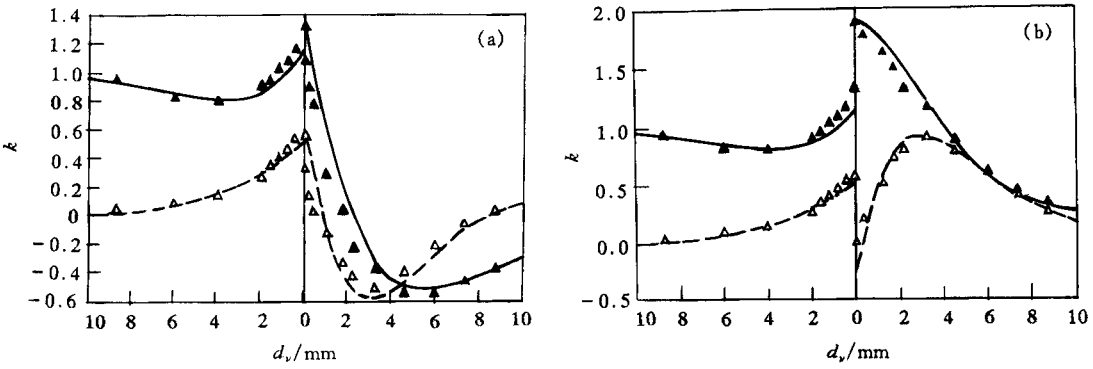

Fig. 5. (a) Distribution of k along the gage line $\theta = 90°$ on the outer surface of a model ($\rho_0 = 0.8$) for M_{xc}. (b) Distribution of k along the gage line $\theta = 90°$ on the inner surface of a model ($\rho_0 = 0.8$) for M_{xc}. - - -, k_ν analytic; ——, k_t analytic; △, k_ν tested; ▲, k_t tested.

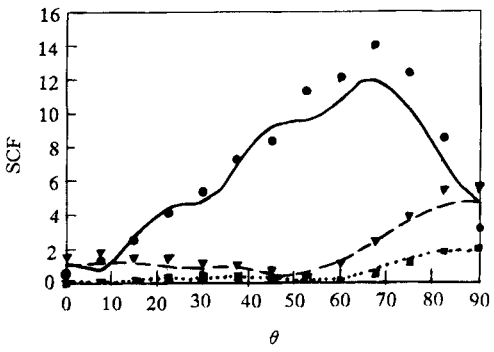

Fig. 6. SCF for varying θ along the crotch line on the inner surface of cylinder. ●, M_{xc} (numerical); ——, M_{xc} (analytic); ▼, M_{yc} (numerical); - - -, M_{yc} (analytic); ■, M_{zc} (numerical), ·····, M_{zc} (analytic).

4.2 Comparison with Moffat's FEM results

Moffat gave a number of numerical results[6,7] and stress concentration factor diagrams for $\rho_0 \leqslant 1$, $D/T \leqslant 70$ and $\rho_0 \leqslant t/T \leqslant 1$ based on 3D-finite element method. The comparison between the present and Moffat's results for $\rho_0 = 0.8$, $D/T = d/t = 40$ under three cases (see fig. 6) shows that the two results of SCF versus θ are in good agreement. Here, SCF is the dimensionless Tresca stress intensity and usually SCF along the crotch line on the inner surface of cylinder is the maximum compared with those on the outer surface. The comparison of relations of maximum dimensionless Tresca stress intensity, K_{xc}, K_{yc} and K_{zc}, to ρ_0 and $D/T = d/t$ with Moffat's results given in figs. 7(a)—(c) shows that they are in good agreement as well. Here, subscript K means the loading case.

5 The relation of K to ρ_0, λ, and t/T

From the above-mentioned analysis the maximum dimensionless stress intensity, K, is de-

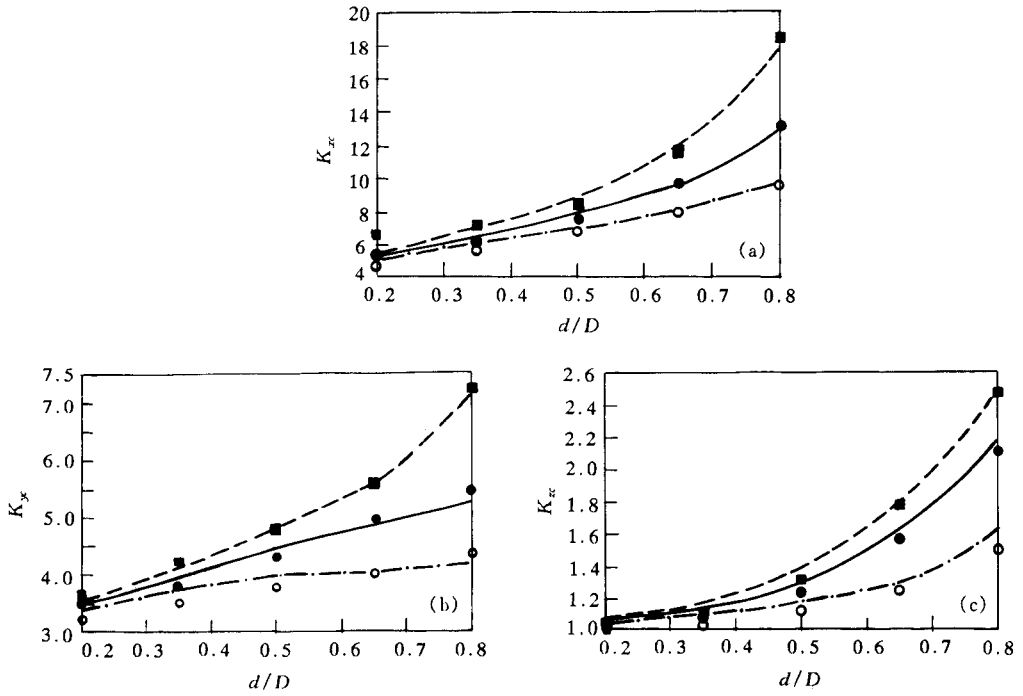

Fig. 7. (a) Maximum of SCF(K_{xc}) for varying d/D and D/T due to torsional moment M_{xc}. (b) Maximum of SCF (K_{y}) for varying d/D and D/T due to in-plane moment M_{y}. (c) Maximum of SCF(K_{zc}) for varying d/D and D/T due to out-plane moment M_{zc}. - · - ·, $D/T=20$ (this paper); ——, $D/T=40$ (this paper); - - - -, $D/T=60$ (this paper); ○, $D/T=20$ (Moffat[6]); ●, $D/T=40$ (Moffat[6]); ■, $D/T=60$ (Moffat[6]).

pendent on the parameters $\rho_0 = r/R$, $\lambda = (d/D)\sqrt{D/T}$ and t/T. A set of design diagrams can be given by the present analytical method. An example of K_{xc} for $\rho_0 = 0.8$, $2.5 \leqslant \lambda \leqslant 8$, $\rho_0 \leqslant t/T \leqslant 2$ is shown in figure 8.

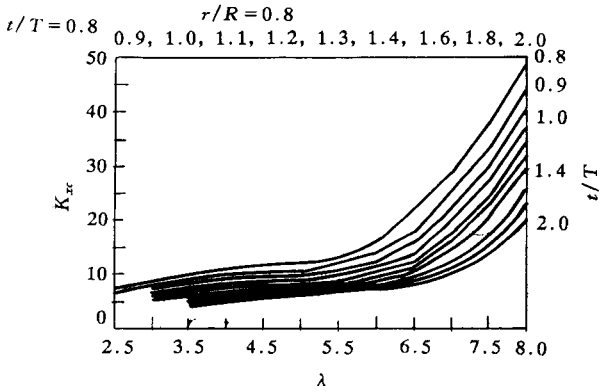

Fig. 8. Maximum of SCF (K_{xc}) for varying λ and t/T due to torsional moment M_{xc} on cylinder.

6 Conclusion

A thin shell theoretical solution of cylindrical shells with normally intersecting nozzles due to external moments on the ends of shells is given in this paper. The solution applicable to $r/R \leqslant$

0.8 is successful by experimental and numerical verification.

References

1 Eringen, A. C., Naghdi, A. K., Thief, C. C. et al., Stress distribution at two normally intersecting cylindrical shells, *Nuclear Structural Eng.*, 1965, 2: 235.

2 Bijlaard, P. P., Stresses from local loading in cylindrical pressure vessels, *Trans. ASME*, 1955, 77: 805.

3 Qian, L. X., Tan, X. J., Zhong, W. X. et al., General solution of cylindrical shells with a cut-out, *J. Dalian Inst. Technol.* (in Chinese), 1965, 3(4): 1.

4 Lekerkerker, J. G., The determination of elastic stresses near cylinder-to-cylinder intersection, *Nuclear Eng. Des.*, 1972, 20: 57.

5 Steele, C. R., Steele, M. L., Stress analysis of nozzle in cylindrical vessels with external load, *ASME J. Pres. Ves. Tech.*, 1983, 105: 191.

6 Moffat, D. G., Mwenifumbow, J. A. M., Xu, S. H. et al., Effective stress factors for piping branch junctions due to internal pressure and external moment loads, *J. of Strain Analysis*, 1991, 26(2): 85.

7 Amran, B. A., Moffat, D.G., Mistry, J., Interaction of pressure and moment loads on a piping branch junction using finite element analysis, *Proc. 8th Int. Conf. on Pres. Ves. Technology*, Vol. 2, Design and Analysis, Montreal, ASME, 1996, 185—196.

8 Afshari, P., Widera, G. E. O., Analysis of shell intersections, *Int. Conf. of Pres. Ves. Tech.*, 1991, 378.

9 Xue, M. D., Deng, Y., Hwang, K.C., Some results on analytical solution of cylindrical shells with large opening, *ASME J. Pres. Ves. Tech.*, 1991, 113: 297.

10 Deng, Y., Hwang, K. C., Xue, M.D., The stress analysis of cylindrical shells with rigid inclusions having a large ratio of radii, *SMiRT* 11 *Transactions F*, F05/2, Tokyo, 1991, 85—90.

11 Xue, M. D., Chen, W., Deng, Y. et al., The thin shell theoretical solution for cylindrical shells with large openings, *Acta Mechanica Sinca* (in Chinese), 1995, 27(4): 482.

12 Xue, M. D., Chen, W., Hwang, K. C., Stresses at the intersection of two cylindrical shells, *Nuclear Engineering and Design*, 1995, 154: 231.

13 Xue, M. D., Hwang, K. C., Lu, W. et al., A reinforcement design method based on analysis of large openings in cylindrical pressure vessels, *ASME J. Pres. Ves. Tech.*, 1996, 118: 502.

14 Timoshenko, S., Woinowsky-Krieger, S., *Theory of Plates and Shells*, New York: Mc Graw-Hill Book Company, 1959.

15 Goldenveizer, A. L., *Theory of Elastic Thin Shells*, New York: Pergamon Press, 1961.

16 Hwang, K. C., Lu, M. W., Xue, M. D., *Theory of Thin Shells* (in Chinese), Beijing: Higher Education Press, 1988.

17 Corum, J. M., Bolt, S. E., Greenstreet, W. L. et al., Theoretical and experimential stress analysis of ORNL thin shell cylinder to cylinder Model-1, *ORNL Report* 4553, 1974.